Directive 2-D Beam Steering by Means of a Multi-Port Radially Periodic Leaky-Wave Antenna

Directive 2-D Beam Steering by Means of a Multi-Port Radially Periodic Leaky-Wave Antenna

Davide Comite, *Senior Member, IEEE,* Maksim Kuznetcov, *Student Member, IEEE,* Victoria Gómez-Guillamón Buendía, *Member, IEEE*, Symon K. Podilchak, *Member, IEEE*, Paolo Baccarelli, *Member, IEEE,* Paolo Burghignoli, *Senior Member, IEEE,* and Alessandro Galli, *Member, IEEE*

***Abstract*—A multi-fed radially periodic two-dimensional leaky-wave antenna is proposed for the generation of a directional beam continuously scanning in *elevation* by changing the frequency, and over a discrete number of directions in *azimuth* when activating different elements of the feeding system. The structure is planar and constituted by a circular grounded dielectric slab loaded with microstrip rings, properly positioned around the sources to support the propagation of an angularly directional surface wave over a sector determined by the corresponding activated feeder. This produces a perturbation of the surface wave, resulting in the generation of a directional leaky wave over the aperture, whose complex propagation constant is described by a single fast *backward* spatial harmonic. The antenna radiation features are numerically investigated in conjunction with the dispersion analysis of the structure, validated through a conventional generalized-pencil-of-function approach. Full-wave simulations have been developed to design a practical feeder, which is constituted by a circular arrangement of commercial coaxial connectors. The proposed multi-port antenna is validated by means of measurements performed on a microwave manufactured prototype. The design represents an attractive simple and cost-effective solution to achieve a high-gain beam scanning over the three-dimensional space, alternative to more conventional phased-array design based on cumbersome and lossy feeding networks.**

***Index Terms*—Beam steering, leaky-wave antennas, antenna arrays, pencil beams, tapered leaky waves.**

I. Introduction and Motivation

REMOTE sensing applications, wireless power-transfer systems, and localization devices often demand for the generation of high-gain beams through compact, integrated, and cost-effective antenna designs. Established techniques for generating high-gain pencil beams scannable or steerable over the three-dimensional space are based on the design of arrays of planar radiating elements with low or moderate directivity. Most common solutions typically involve patch antennas, singularly activated or arranged in series to enhance the directivity of the single element [1]. Phased arrays, however, require the use of feeding networks to control the excitation coefficients at the input ports. Digital beam-scanning technique are nowadays well established, but they involve lossy and bulky structures. More importantly, the corresponding feeding networks can be very complex and expensive [2].

An alternative, well-established, solution to achieve directional beams scanning with frequency in elevation is based on one-dimensional (1-D) and two-dimensional (2-D) leaky-wave antennas (LWAs) [3], [4]. The former enables the radiation of a high-gain fan beam leveraging on the excitation of an aperture field having exponential decay along one longitudinal direction; the latter, depending on the geometrical symmetry enforced by the feeder, radiates a conical omnidirectional or conical sector beam supported by the excitation of a cylindrical leaky wave (LW). Over the last few decades, different solutions based on LWAs have been proposed to design high-gain beam scanning over the three-dimensional (3-D) space. This can be achieved by arranging LW line-source antennas into linear arrays, therefore including phase shifters in only one dimension [5]-[8], or by embedding a reduced number of sources within a Fabry-Perot cavity antenna (FPCA) [9].

LWAs fed with array structures have received considerable attention over the last decade [10]-[13]. They have been demonstrated to improve the gain of thinned arrays radiating at broadside [10], [14], and, more recently, to enhance the coverage of a multibeam system [15]. A study about the capability of enhancing the antenna aperture efficiency has been presented in [16], whereas a LW thinned design for grating-lobe reduction has been proposed in [17]. A frequency-scanned monopulse radar using an array of two LWAs has been proposed in [18]. Metasurface antennas excited by multiple feeds to achieve multibeam and beam-scanning capabilities have been proposed in [19], [20]. Finally, some of the present authors proposed in [21] a 2-D LWA fed by four surface-wave launchers placed in the antenna center to provide full polarization reconfigurability.

The possibility of obtaining scannable beams at a fixed frequency using FPCAs has been explored by electronically reconfiguring the partially reflecting surface on top, both in 1-D [22] and 2-D [23]-[25] layouts, also exploiting two phased patches as feeding system of the structure [26]. A method to steer the beam of an aperture antenna based on a near-field phase transformation have been proposed in [27], [28], whereas a phase-modulated metasurface has been presented in [29].

Davide Comite, Paolo Burghignoli, and Alessandro Galli are with the Department of Information Engineering, Electronics and Telecommunications, "Sapienza" University of Rome, 00184 Rome, Italy (e-mail: davide.comite@uniroma1.it).

Maksim Kuznetcov and Symon K. Podilchak are with the Institute of Digital Communications, The University of Edinburgh, Edinburgh EH14 4AS, UK.

Victoria Gómez-Guillamón Buendía is with the Institute of Sensors, Signals, and Systems, School of Engineering and Physical Sciences, Heriot-Watt University, Edinburgh, EH14 4AS, UK.

Paolo Baccarelli is with the Department of Engineering, "Roma Tre" University, 00146 Rome, Italy.

Manuscript received May 4th, 2020.

More recently, in [9], some of the present authors investigated the advantages achievable by exploiting a directional element radiation pattern obtained embedding an array inside a planar FPCA. The work demonstrated the possibility of achieving a high-gain pencil-beam scanning both in azimuth and elevation by properly *phasing* the array of the azimuthally invariant sources and changing the frequency, respectively. Such an uncommon feature was enabled by the excitation of a dominant cylindrical TM LW of 0−th azimuthal order [30]. The structure in [9] was bounded on top by a *homogenized partially reflecting surface*, representing one of the key aspects of the approach. Its subwavelength and translational invariant nature, indeed, permits to freely select the sources position and spacing within the cavity, as well as to perform the dispersive analysis by means of the definition of an equivalent transverse network (see [31] and refs. therein). This is achieved with a structure having thickness in the order of half a wavelength, which requires the use of spacers or the design of stacks of multilayer dielectric laminates, preventing thus the use of conventional PCB approaches for a complete integrability with other circuitry. Nonetheless, FPCA antennas fed by azimuthally symmetric sources can suffer the undesired excitation of a quasi-TEM mode [31], which unavoidably degrades the radiation efficiency and, if its radiation regime is not properly suppressed, determines the presence of a spurious lobe close to endfire [9], [32].

To overcome these limitations and to provide 2-D steering capabilities with a compact structure based on conventional single-layer PCB technology, we propose here the design of a 2-D radially periodic LWA fed by a circular arrangement of vertical coaxial probes (see Figs. 1(a), (b) and 2), whose radial distance, size, and position is optimized to excite an angularly directional surface wave (SW) around the main direction dictated by the corresponding source of the multi-port system, which, as opposed to the phased-array in [9], are activated therefore one at time defining a multi-port antenna. The presence of a periodic perturbation determined by the *metallic annular grating* allows for transforming the directional SW into a LW, which, if properly designed, still represents the dominant contribution to the directional aperture field supported by the structure, and whose radiation can be described by a single fast backward spatial harmonic. This results in a high-gain pencil beam radiating off broadside, scanning with the frequency in elevation and steerable over a discrete number of azimuth directions (defined by the number of sources of the multi-port system), in contrast with the high-gain omnidirectional conical beam achievable by placing the same source in the geometrical center of the structure [33].

The working principle of the proposed structure, completely different with respect to the alternative LWA planar design based on a FPCA [9] because of the lack of translational symmetry, is described in the following by means of full-wave dispersive analyses and numerical simulations, whereas its performance is validated through measurements developed on a manufactured prototype.

This paper is organized as follows. Sec. II presents the main theoretical background for the description of the field distribution in conjunction with the relevant dispersive analysis,

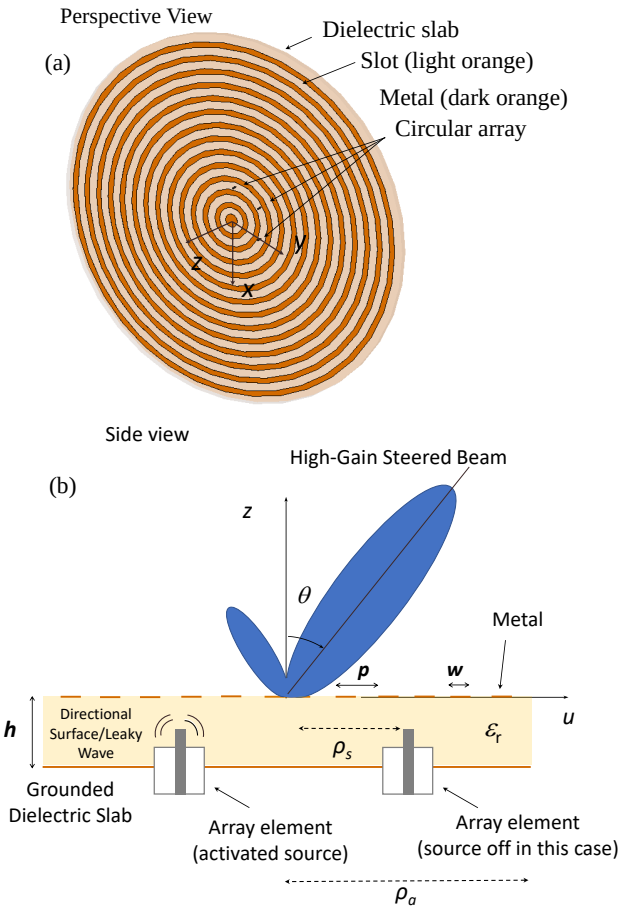

Fig. 1. Perspective (a) and side (b) views of the multi-port planar antenna made by a radial microstrip ring arrangement on a grounded dielectric slab (GDS). The u axis represents an arbitrary radial cut of the annular structure. ρ_a and ρ_s represent the radial extension of the antenna and of the circular feeding system, respectively.

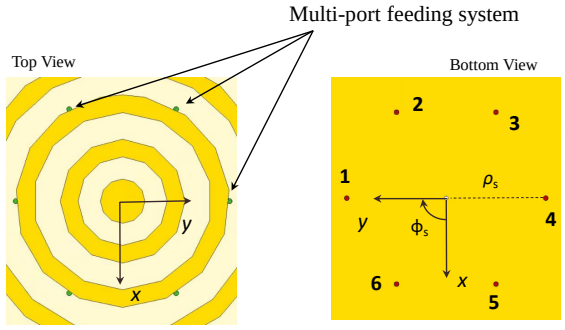

Fig. 2. Zoomed top and bottom views of the multi-fed planar LWA. The angular position of the sources, ϕ_s, is measured with respect to the x axis.

whereas Sec. III reports some numerical studies on the far-field features of the antenna. Sec. IV reports the results of the experimental characterization obtained through measurements of a manufactured prototype IV. Final discussions and conclusions are drawn in Sec. V.

II. Aperture-Field Analysis

As shown in Figs. 1(a), (b), the antenna is fed by a circular arrangement of coaxial probes (zoomed in Fig. 2), activated

one at time with the same amplitude and arbitrary phase to enable the generation of a high-gain pencil beam at an elevation angle dictated by the frequency, and at an azimuth angle that corresponds to the angular position of the probes within the circular feeding system (described by ϕ_s in Fig. 2, right panel). In this case, only a discrete number of pointing angles can be covered but without requiring the use of complex feeding networks to phase the sources.

To describe the physical mechanism enabling the generation of the pencil beam, in the following, we study the SW excited by a non-centered vertical coaxial probe in the presence of one and two printed microstrip rings. The radial position of the source is optimized to strongly excite two internal rings, thus defining a SW mainly focused around the azimuth direction controlled by ϕ_s.

A. Surface-Wave Excitation

Let us consider a finite circular radiating aperture of radius ρ_a orthogonal to the z-axis of the system with its origin ($\rho = 0$) at the aperture center (see also Fig. 1). For simplicity, we consider the same structure designed to support a scanning conical beam [33] and to launch a Bessel beam [34], constituted by an annular GDS having thickness $h = 3.14$ mm having permittivity $\varepsilon_r = 2.2$, fed by a vertical coaxial probe protruding through the ground plane. By following the design of similar planar-periodic LWAs, [33] and [35], the feeder can be placed at a certain distance from the top strips to control the radiation features and port matching.

To assess the possibility of radiating a directional pencil beam off broadside, keeping the azimuth symmetry of both feeder and GDS, we analyze the aperture field of the structure constituted by one and two annular rings excited by a vertical short dipole on the ground plane placed at a radial distance equal to ρ_s. Figs. 3(a)-(c) report the transverse component of the time-harmonic normalized electric field (i.e., $|\mathbf{E}_t| = \sqrt{|E_x|^2 + |E_y|^2}$), simulated with CST microwave studio at a frequency $f = 18$ GHz (selected to be in the propagation regime for the TM_0 supported by the corresponding GDS), sampled at a distance equal to $\lambda/10$ from $z = 0$ (calculated at 18 GHz) from the aperture, for three different structures. A GDS not loaded with any ring in case (a), a GDS loaded with one metal ring having inner and outer radius $r_{1_{i,o}} = 20$ and 24 mm, respectively, in case (b), and one with an additional metal ring in case (c) (the second ring having inner and outer radius $r_{2_{i,o}} = 30$ and 34 mm, respectively). In all cases the source is at $\rho_s = 26$ mm (indicated with a white circle), i.e., in proximity of the two rings, and the radial extension of the overall structure is $\rho_a = 140$ mm.

In the absence of rings (i.e., Fig. 3(a)), the SW field produced by the non-centered source is a TM field with respect to z (the axis being defined at the geometrical center of the structure), and it shows a maximum at the point of the surface directly on top at the source location. This corresponds to the point from which the field spreads as a cylindrical wave in all directions, before being reflected at the truncation (note that the SW slowly attenuates as $1/\sqrt{\rho}$), whose contribution to the total field generates the strong interference pattern. Basically,

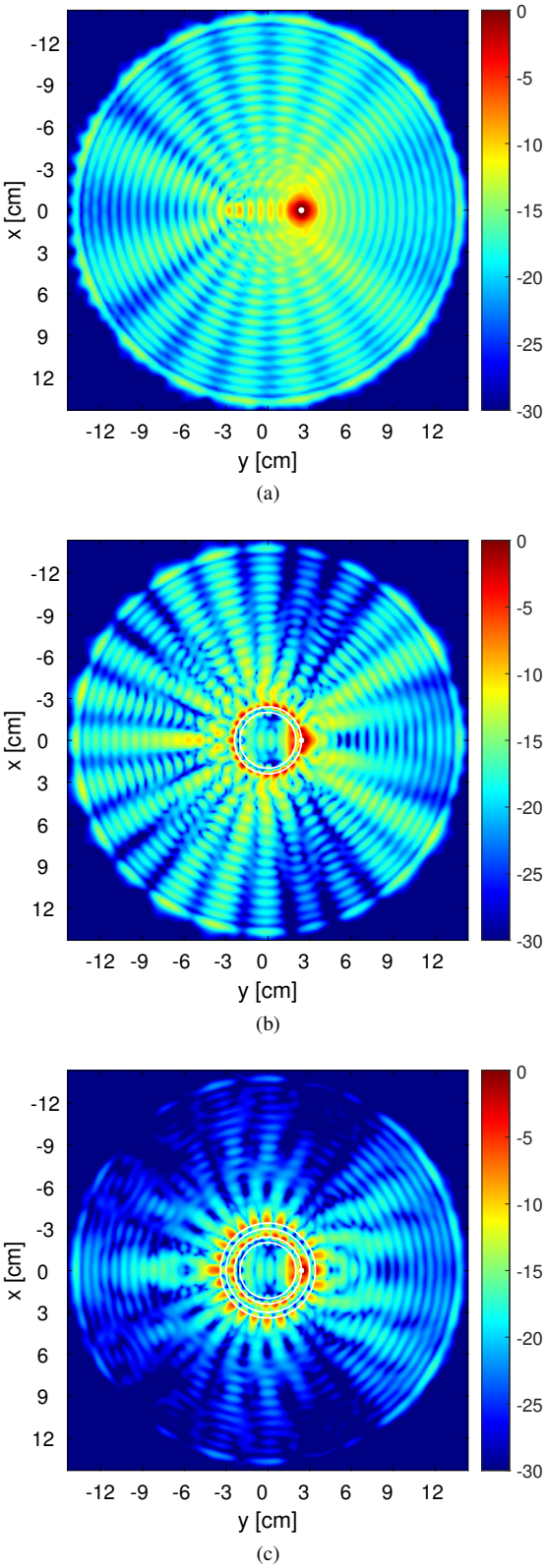

Fig. 3. Transverse field component (with respect to z) of the full-wave time-harmonic aperture field (in dB), at 18 GHz, supported by the GDS when excited by a vertical probe placed at radial distance equal to $\rho_s = 26$ mm: a) GDS not loaded with metal ring; b) GDS loaded on top with one metal ring sized to be placed in proximity of the sources; c) GDS loaded on top with two metal rings sized to be placed around the source. The excitation is reproduced here by considering a short vertical eletric dipole placed on the ground plane (i.e., at $z = -h$). The metal rings are indicated with white solid lines. Structure parameters: GDS thickness $h = 3.14$ mm, permittivity $\varepsilon_r = 2.2$.

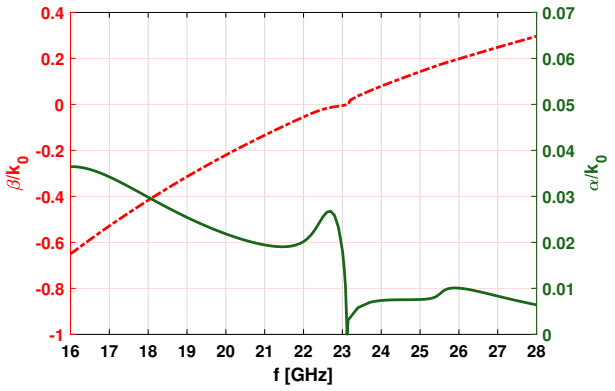

Fig. 4. MoM dispersion behavior for the normalized phase and leakage constants of the linear MSG. The $n = -1$ radiating space harmonic is first in a backward regime (from 16 to about 23 GHz) and then in a forward regime (from about 23 to 28 GHz and beyond). Structures parameters: strip width $w = 4$ mm and period $p = 10$ mm. Other parameters as in Fig. 3.

the SW field is not perfectly omnidirectional, but has some ϕ-dependent TM field distribution.

With the addition of the single metallic ring in Fig. 3(b) a hybrid field is produced, as a result of the scattering from the microstrip ring which is strongly excited. It should be highlighted that, even though for this single-ring case the field loses its omnidirectional behavior, the desired directional pattern for the SW is not satisfactorily defined. In contrast, when the source is positioned at the origin for SW excitation, as in [33], similar strong microstrip ring excitation is not observed. In this case, radiation is purely defined by the dominant TM LW mode achieving conical radiation without any spurious effects which are related to these microstrip rings modes [36].

The presence of a second ring (Fig. 3(c)) produces further considerable scattering, resulting in a concentrated SW field around the azimuth direction controlled by the source ($\phi_s = 90°$ in this case).

The azimuth symmetry of both the feeder and structure assures the same SW field distribution, which changes with the value of ϕ_s. This in as essential feature to steer the far-field beam by means of a multi-port excitation when considering the complete LWA (see Fig. 2).

As it will be discussed in the following, the directional SW can be perturbed to achieve directional radiation by means of a LW, whereas more feeders can be placed along the circle drawn by the source to steer the SW and, therefore, the corresponding beam. It should be emphasized that the position of both feeder and ring have been properly tuned, but no significant performance improvements have been observed by changing the ring dimension and position around the source. More involved strategies could be considered to improve the directional pattern of the SW, but, to steer the beam over the entire azimuth plane in the far-field, the symmetry of the annular metal strip grating (MSG) has to be maintained.

B. Dispersion Analysis

Introducing a periodic perturbation to the SW supported by the structure in Fig. 3(c), a directional pencil beam scanning with frequency can be, in principle, achieved. This can be straightforwardly verified by letting radiate (by means of a conventional FFT operation) a transverse, non-truncated, aperture field given by the following expression

$$E_\rho(\rho, z = 0) = -j\frac{k_z}{k_\rho} A(\phi) H_0^{(1)'}(k_\rho \rho) \tag{1}$$

where $H_0^{(1)'}(\cdot)$ is the first-order derivative of the zeroth order Bessel function of the first kind with respect to its argument, k_ρ and $k_z = (k_0^2 - k_\rho)^{1/2}$ are the transverse and vertical wavenumbers associated with the aperture field; k_0 is the free-space wavenumber and $A(\phi)$ is an amplitude function describing the azimuth dependence of the field, which also includes the complex constant factor E_0 related to the excitation.

If the structure is excited in the center with an azimuthally symmetric feeder, the directional tapering enforced by $A(\phi)$ in (1) vanishes and the apertured field can be described by a single, zeroth-order, harmonic, as discussed in [33], [34]. The use of non-centered sources, in general, determines the excitation of higher-order (i.e., with $n > 0$) harmonics. Thanks to the lack of translational invariance of the structure, such higher azimuthal harmonics may combine to produce directional radiation, as discussed next.

Assuming a directional behavior of $A(\phi)$ around $\phi_s = 90°$, a pencil-beam scanning with the frequency in the far field can be achieved, which is directed along the elevation angle dictated by conventional LW theory (assuming therefore k_ρ as the radial wavenumber of the corresponding cylindrical LW). Note that, in the following, a local maximum over the aperture will be also observed at $\phi = \phi_s + 180°$.

On this basis, to transform the SW in Fig. 3(c) into a directional LW, while keeping the needed azimuth symmetry, we consider here an annular metallic strip grating as in [33], which can be simply achieved by completing the sequence of annular rings initiated by the original two (as in Fig. 3(c)) positioned to establish a directional SW.

We consider the GDS of Sec. II-A and results are reported in Fig. 4. By local linearization of the radially periodic structure in Fig. 1, we can represent the radial field distribution as a wave propagating along a 1-D periodic MSG [33], thus described in terms of space harmonics (Floquet waves) [4]. Assuming a direction of propagation along the y-axis of the linearized structure (see Fig. 1), the n-th space harmonic has a wavenumber defined by $k_{yn} = k_{y0} + 2\pi n/p$ where p is the radial period and $k_{y0} = \beta_0 - j\alpha$ is the wavenumber of the fundamental harmonic [4] (β_0 and α being the phase and attenuation constant, respectively).

Thanks to this local linearization within the unit cell, one can assume that $k_{\rho n} = k_{yn}$, which is the transverse wavenumber of a cylindrical wave associated with the n-th space harmonic [30], [33]. This approach has been proved to be accurate to describe both the far field [33], [36] and the near field [34].

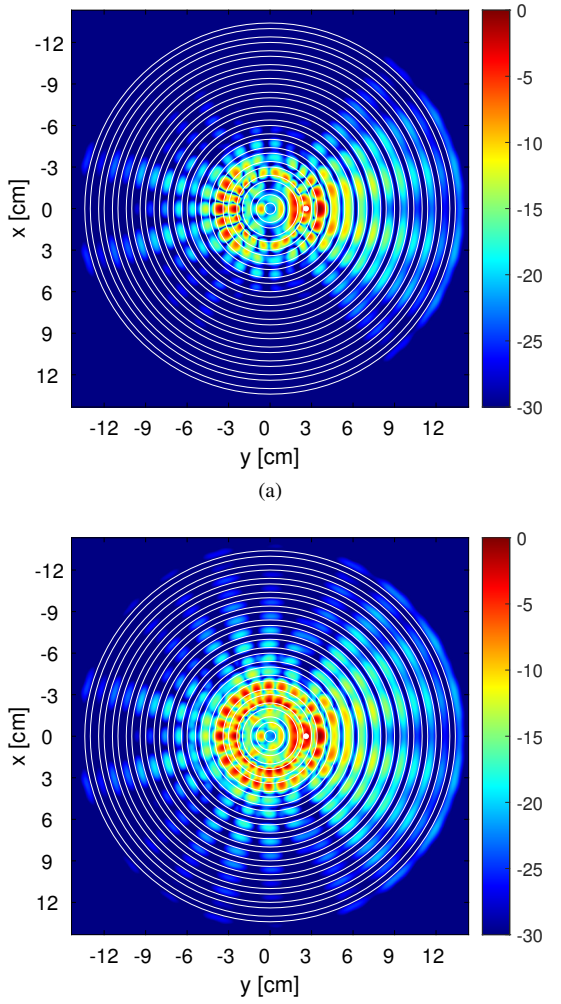

Fig. 5. Aperture field, at 18 GHz, supported by the LWA when excited by a vertical probe placed at $\rho_s = 26$ mm: a) E_y component (in dB) of the aperture field; b) transverse component (in dB) with respect to z. The source position is the same as in Fig. 3. There are 14 annular metal rings ($\rho_a = 280$ mm), indicated by the white rings. The most internal ring of the structure has zero inner radius.

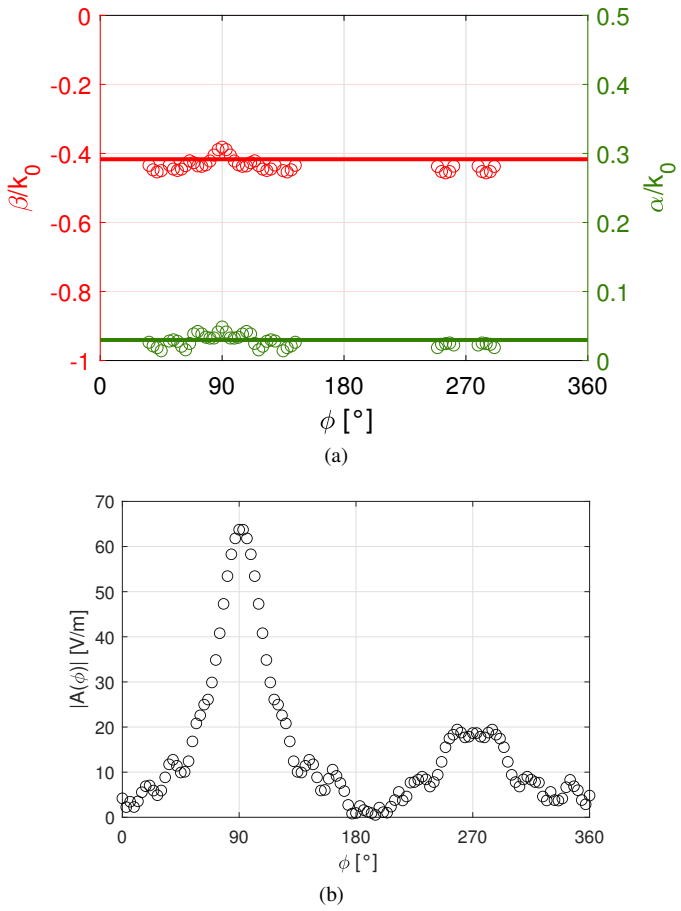

Fig. 6. (a) Normalized phase and attenuation constant of the leaky mode at 18 GHz retrieved by means of the GPOF applied to the simulated aperture field in Fig. 5(a). The solid lines report the expected theoretical value from Fig. 4; (b) Absolute value of the complex amplitude coefficient of the corresponding complex exponential retrieved by the GPOF.

The original GDS and the metal strips in [33] are designed to operate in a frequency range where a fast space harmonic exists (e.g., the $n = -1$) with a suitable attenuation in the backward region, thus defining a proper LW with $\beta_{-1} < 0$. If excited in the center of the structure, the space harmonic will propagate as an attenuated outward cylindrical wave with E_ρ proportional to $H_0^{(2)\prime}(k_{\rho,-1}\rho)$, where $k_{\rho,-1} = \beta_{-1} - j\alpha_\rho$, with $\beta_{-1} < 0$ and $\alpha_\rho > 0$. Following conventional LW theory [3], the main beam pointing angle is related to the LW phase constant β_{-1}, i.e., $\theta_p^{LW} \approx \sin^{-1}(\beta_{-1}/k_0)$. We will assume, in the following, that the wavenumber of the LW associated with the spatial harmonic can still accurately describe the directional aperture field established on the structure in Fig. 3(c) completed with all rings (as in Fig. 1(a)). This assumption will be validated by means of full-wave simulations and a dispersive analysis performed by means of a conventional generalized-pencil-of-function (GPOF) approach [37].

To retrieve firstly the LW complex propagation wavenumber $k_{\rho,-1}$ supported by the structure, we considered the dispersive analysis in [33], developed by means of an in-house method-of-moments approach. The corresponding normalized phase and attenuation constant are reported in Fig. 4. A good (rather less than unity) normalized leakage constant, in the order of 0.03, is achieved in the backward region around 18 GHz.

C. Leaky-Wave Aperture Field and GPOF Analysis

In this section, we investigate the aperture field of the GDS loaded with an annular MSG defined by 14 microstrip rings, fed by an individual non-centered ideal source (similar to Fig. 3(c)). In this study, for comparison, the source is placed at two different radial distances $\rho_s = 26$ mm and $\rho_s = 36$ mm.

Figures 5(a), (b) report the y component and the transverse component (with respect to z) of the normalized aperture field for $\rho_s = 26$ mm. The E_y component, reported in Fig. 5(a), shows an aperture field well focused around the direction dictated by the source position (i.e., $\phi_s = 90°$ as in Fig. 3). Therefore, a desired directional behavior of the aperture field is achieved, whose description by means of the expression in (1) will be discussed in the following. Fig. 5(b) confirms the expected directional behavior of the aperture field.

To assess the nature of the aperture field in Fig. 5 we analyze the y component by means of a GPOF approach

[37], [38], which essentially allows for numerical retrieving both amplitude (A(ϕ) in (1)) and phase (i.e., the complex propagation constant of the leaky mode) of the complex exponentials that decompose the field along an arbitrary radius and, in particular, around the direction $\phi_s = 90°$. To this aim, to match the field dependence expressed by the Hankel function in (1)), we consider the aperture field starting at $\rho^{\text{GPOF}} = 4$ cm (same performance can be obtained changing this point, provided that $\rho^{\text{GPOF}} \geq \rho_s$) and compensate for the attenuating factor $1/\sqrt{\rho}$ typical of a cylindrical wave. In this way, the retrieved complex exponential can be compared with the well-known asymptotic expansion of the Hankel function.

Figure 6(a) reports the phase (left axis) and the attenuation (right axis) constant estimated at 18 GHz by means of the GPOF algorithm versus the azimuth angle ϕ. The theoretical value of the $n = -1$ fast spatial harmonic in Fig. 4, i.e., $k_{\rho,-1}^{\text{LW}} = k_{y,-1}^{\text{LW}} = (-0.42 - j0.03)k_0$, has been also reported for comparison. Only values associated with a fitness function R_f, defined as follows, greater than 0.9 have been reported

$$R_f = 1 - \frac{\sum_\rho |E_y^{\text{CST}} - E_y^{\text{GPOF}}|^2}{\sum_\rho |E_y^{\text{CST}} - \hat{E}_y^{\text{CST}}|^2} \tag{2}$$

where $\hat{E}_y$ is the mean value of the field over the considered antenna aperture plane and $E_y^{\text{GPOF}} = A(\phi)e^{-j(\beta^{\text{GPOF}} - j\alpha^{\text{GPOF}})\rho}$. CST refers to the field achieved by numerical computation. A very good agreement between the theoretical dispersive analysis and the GPOF estimation is visible in Fig. 6 around the radial region where the source is located and the aperture field in Fig. 5 is well defined. Same for the narrower region located at the opposite direction (i.e., for $\phi = 270°$).

Figure 6(b) reports the magnitude of the complex amplitude coefficient estimated by the GPOF. The curve shows a maximum value around ϕ_s and a local maximum at the opposite direction, as expected. These results confirm the accuracy of the proposed LW model to describe the angularly directional aperture field supported by the structure.

We also analyzed the same structure with radius $\rho_s = 36$ mm (results not shown here for brevity). We observed an improved directional behavior with respect to those in Fig. 5(a), (b) since the source is moved one period away from the center but two more annular rings were added, defining a radial aperture having size $\rho_a = 320$ mm (contrasted with $\rho_a = 280$ mm for the antenna in Fig. 5). Keeping unchanged the attenuation constant of the LW (i.e., keeping the same period and strip width), the presence of more rings reduces the interference effect mainly generated by the LW reflected at the truncation. The GPOF algorithm was also applied showing very good agreement with the theoretical values of the phase and the attenuation constants. The magnitude of the complex amplitude coefficient estimated as in Fig. 6(b) showed, again, a curve having its maximum value around ϕ_s and a local maximum in the opposite direction, confirming the accuracy of the LW model.

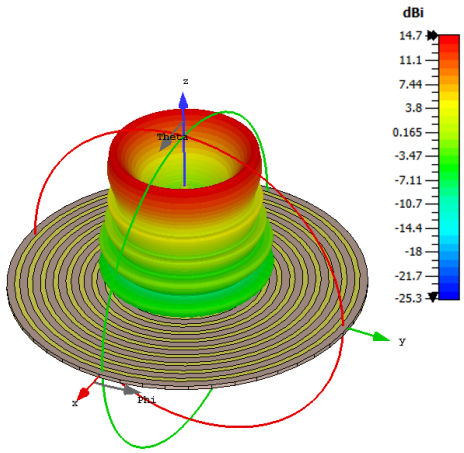

Fig. 7. 3-D directivity of the conical beam pattern radiated by the source placed in the center, at $f = 18$ GHz. Thanks to the azimuthal symmetry of both the source and guiding structure the polarization of the radiated beam is purely vertical.

III. Far-Field Features

A. Feeding System Design and Positioning

An important feature of LWAs is their low-profile and low-cost nature as well as the possibility of being excited by a simple and integrated system. This is in contrast with more complicated feeding networks needed, e.g., by phased-array configurations. To feed the directional SW we use here a vertical 50-Ω coaxial probe. If placed in the center, the probe couples with the vertical component of the field inside the GDS to launch an outward TM cylindrical wave, which is transformed into a LW with a backward $n = -1$ spatial harmonic by the MSG. The 3-D directivity of the resulting radiation pattern at $f = 18$ GHz is reported in Fig. 7.

As discussed in Sec. II, the field launched by the non-centered probe strongly excites the nearby rings, thus producing a directional SW. This has been verified for two different positions of the probe; the final choice is related to the radial aperture of the structure, as the directional LW, depending on the attenuation constant of the LW mode, needs to be supported by a certain number of periods to propagate away from the source (at least 12-14 in this case). To achieve satisfactory directionality, in this case, the probe positions should be about 25 mm away from the origin (see Fig. 5).

We have modeled in CST Microwave Studio a 50-Ω coaxial cable connector with an inner and outer diameter equal to 0.3 mm and 1 mm, respectively, that penetrates the ground plane. To be coherent with the experimental validation reported next, we consider here $\rho_s = 26$ mm. An arrangement of six probes is considered: to accommodate the internal feed points along with the Teflon insulator, six holes having diameters equal to about 1 mm were drilled into the GDS. The external cladding of each probe were soldered to the ground. The probe penetration inside the cavity was then tuned by means of a parametric analysis with CST to optimize the input 50-Ω matching. The final configuration shows a probe length $L = 3$ mm.

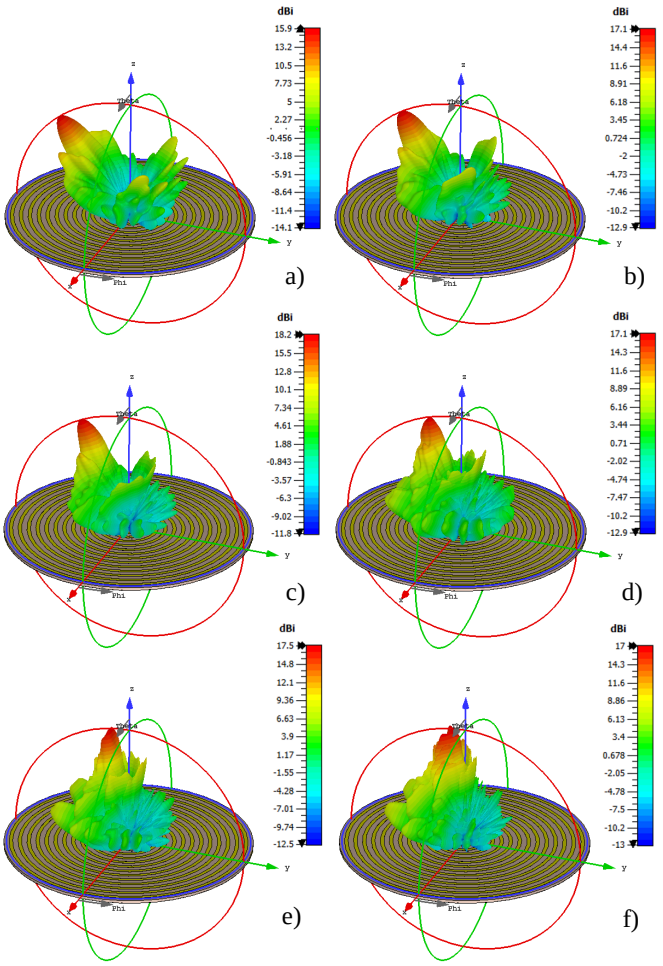

Fig. 8. Simulated 3-D directivity of the LWA excited by a multi-port circular system with one single probe activated (the one placed at $\phi_s = 90°$, i.e., along the y axis). In this case a total of 6 ports were employed (see Fig. 2), driven only by one port. From (a) to (f), the six panels report six frequency values, from 16 GHz (a) to 21 GHz (f).

B. Radiation Pattern

We propose a numerical study of the far-field features of the structure, simulated with CST, exciting the antenna with a circular feeding system of six sources as in Fig. 2, placed at the optimum radius $\rho_s = 26$ mm, thus strongly exciting the 3rd and 4th rings of the periodic structure. More sources could be possibly included depending on the size and the encumbrance of the probes. The probes can be activated one at time and, given the azimuth symmetry of the structure, changing the source (from 1 to 6 in this case, as shown in Fig. 2), the same rotated beam can be achieved in the far-field. Therefore, for brevity, only one case will be considered here.

Figure 8 reports the 3-D directivity of the beam for different values of the frequency (from 16 GHz to 21 GHz, at a step of 1 GHz), achieved by activating the source 1 in Fig. 2. As visible, a well-defined directional pencil-beam scanning with the frequency from a direction close to endfire towards broadside, as dictated by the backward character of the excited leaky mode, has been achieved. Maximum values of the directivity of about 17 dB_i can be observed. The beam is

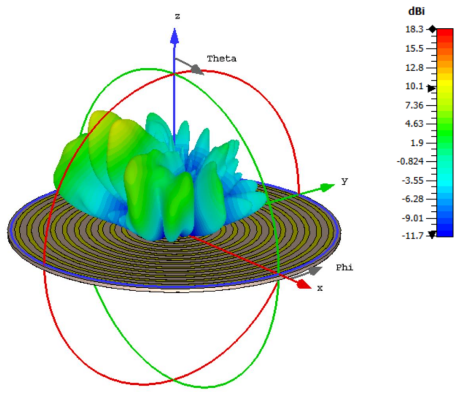

Fig. 9. Simulated directivity of the ϕ component of the field as in Fig. 8, over the 3-D space at 18 GHz. For comparison the dB color scale is as in Fig. 8(c).

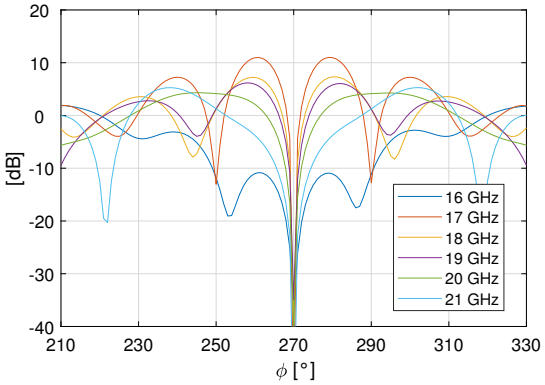

Fig. 10. As in Fig. 9 but over the azimuth cut at $\theta = \theta_p$ (given by the curve in Fig. 12), achieved activating port 1.

vertically polarized (with reference to standard plane-wave polarization definitions) with a good purity around the main direction. However, in contrast with the case in Fig. 7, the non-centered source breaks the azimuthal symmetry producing a hybrid LW aperture field, which generates a cross-polarized component in far field. The ϕ component (reported at 18 GHz in Fig. 9) is well below -30 dB with respect to θ in a region of about 5° around the maximum θ_p^{LW} (note that the plane containing the source is a perfect magnetic wall, where the beam must be vertically polarized), reaching a maximum

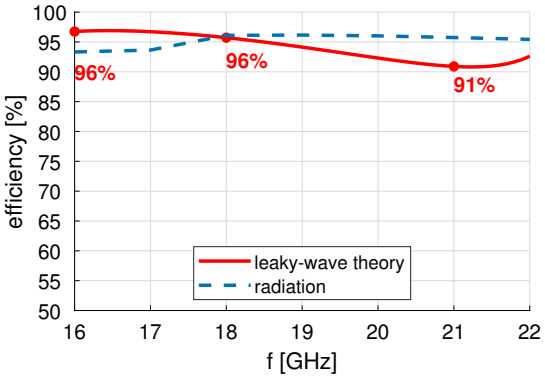

Fig. 11. Radiation efficiency versus frequency for the designed LWA.

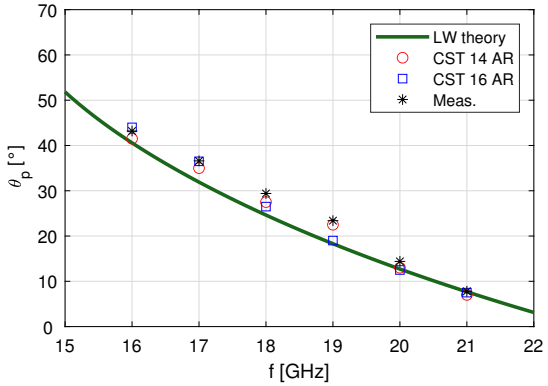

Fig. 12. Comparison between theoretical, simulated, and measured pointing direction θ_p of the pencil beam versus the frequency. Two periodic structures have been considered with 14 and 16 microstrip annular rings (AR).

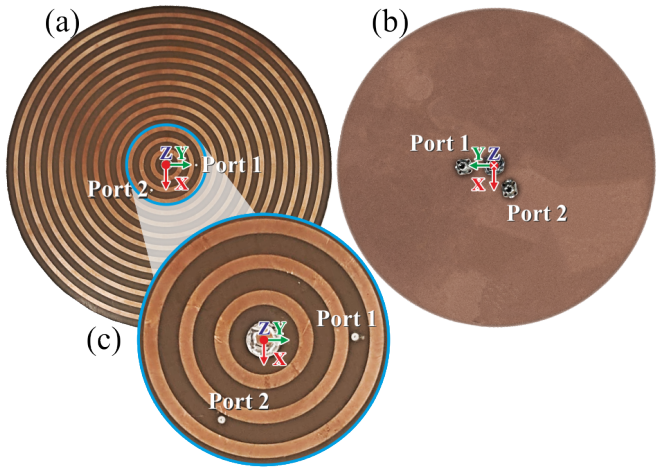

Fig. 13. Top (a) and bottom (b) views of the manufactured prototype for the designed LWA. In (b), the two non-centralized ports are visible, while an additional source is placed in the center to support the radiation of the omnidiretional conical beam in Fig. 7. (c) Zoomed view of the top panel.

value equal to about -10 dB at θ_p^{LW} and $\phi = -\phi_s \pm 5°$). Fig. 10 reports the cross-pol component over the principal plane for the same frequency values as in Fig. 8 (we remind the maximum value of the directivity is about 17 dB_i).

Values of the sidelobe level visible around $\phi = \phi_s$, are about -11 dB at 18 GHz (that is a typical value for a non tapered LWA), and gradually degrade steering the beam towards broadside. The beam never reaches the broadside direction since an open stopband is present (see Fig. 4), which prevents the achievement of sustained leakage around the frequency where $\beta_{-1} = 0$ [39], [40]. In principle, a high-gain pencil beam could be also achieved within the improper frequency region (i.e., for $\beta_{-1} > 0$) where, however, the structure shows a very small attenuation constant.

The theoretical antenna radiation efficiency within the considered frequency range, evaluated with the standard formula based on LW theory ([3], Ch. 7, Eq. 7.28), is also reported in Fig. 11. As expected, the behavior of the red curve reflects the trend of the attenuation constant of the leaky mode supported by the LWA. The radiation efficiency (i.e., accounting for lossy media) evaluated by means of CST is also reported, showing a good agreement.

To give an independent validation of the LW model for the antenna, we propose in Fig. 12 a comparison among the pointing angle of the high-gain beam predicted by the LW theory (i.e., θ_p^{LW}) and those given by CST. A satisfactory agreement has been achieved, coherent with those given by the excitation of an omnidirectional conical beam with a centered probe [33]. This result confirms that the dominant contribution to the far field can be successfully described by a LW aperture field. Further comparisons with measurements will be commented in the next Section.

IV. Experimental Validation

The structure designed and optimized in the previous sections was measured in a calibrated anechoic chamber. A picture of the realized structure is reported in Fig. 13, which shows both top and bottom sides of the manufactured antenna. A zoomed-in top view around the sources is also shown. For proof of concept, and for simplicity, the structure is fed with only two elements of the circular feeding system. It should be also mentioned that a probe was also included in the center for the fabricated structure, mainly for diagnostic purposes during the measurements, probe positioning, and structure mounting. This centralized probe can be employed, as in [33], for conical radiation but it was not examined further in this paper. The $50-\Omega$ coaxial connector are those described in Sec. III-A, whereas the GDS is made on a Taconic TLY5 substrate with permittivity $\varepsilon_r = 2.2$ (tangent loss equal to about $9{\cdot}10^{-4}$ at 10 GHz) and thickness $h = 3.14$ mm.

The y-component of the measured near field radiated by the structure, at a distance $z_0 = 7.8$ cm, is reported in Fig. 14. It is achieved by activating one of the non-centered coaxial probes shown by the bottom panel in Fig. 13. The angularly directional behavior of the field along the y-axis is clearly visible, confirming the behavior of the simulated aperture field reported in Fig. 5.

The simulated and measured reflection coefficients for the two non-centralized probes are reported in Fig. 15(a). Satisfactory agreement and good performance with values below -8 dB within the desired wide frequency range (i.e., from 16 GHz to 21 GHz) can be observed. Figure 15(b) also reports a comparison between the simulated and measured coupling coefficients for the two non-centralized probes (as outlined in Fig. 13), showing good agreement and a maximum value well below -20 dB. It should be identified that the optimization process lacks the needed structure variables to fine tune the impedance matching of the LWA. Due to the non-centralized source, indeed, a variation of the diameter of the first ring of the annular MSG (the one with zero inner radius), as in [33], [34], does not apply here (the pin of the feed does not lie right below and it does not introduce the desired capacitive effect). On the other hand, a fine tuning of the radius of the other annular rings was found to be not effective. More involved strategies could anyway be applied by acting on the geometry of the radial MSG around the source [35], whilst keeping the needed azimuthal symmetry.

Figure 16 reports a comparison between the simulated and

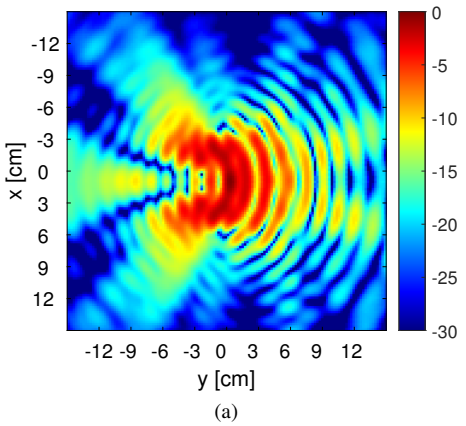

(a)

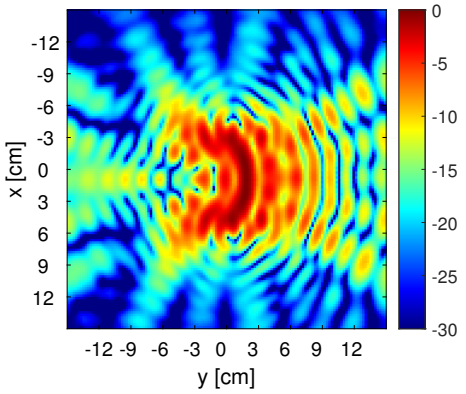

(b)

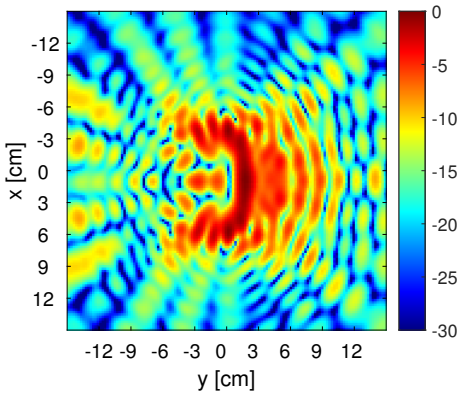

(c)

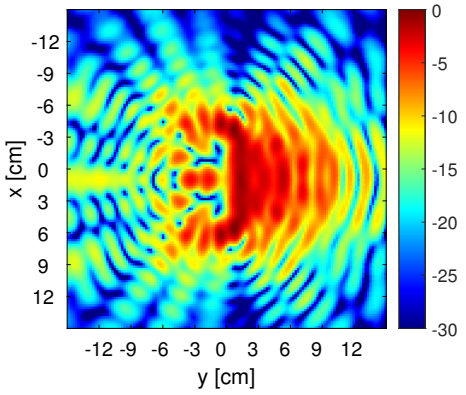

(d)

Fig. 14. Measured near field (E_y in dB) over a plane parallel to the aperture at $z_0 = 7.8$ cm. Four different frequencies have been reported: a) 17 GHz; b) 18 GHz; c) 19 GHz; d) 20 GHz.

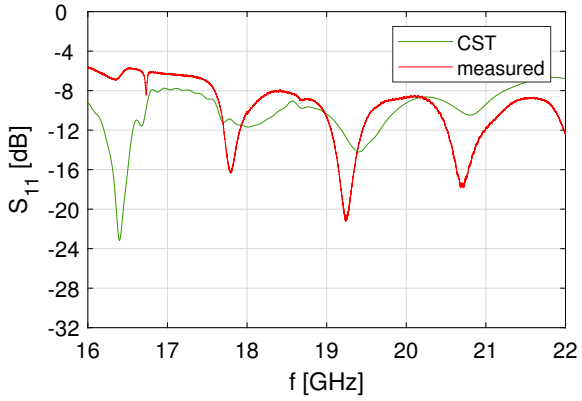

(a)

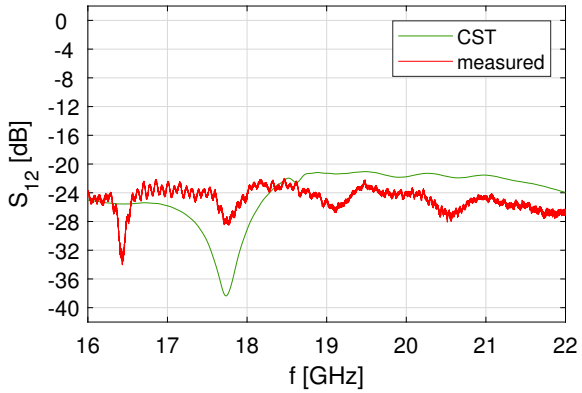

(b)

Fig. 15. (a) Reflection coefficient for port 1 of the simulated and manufactured structure. (b) Coupling coefficient between port 1 and 2.

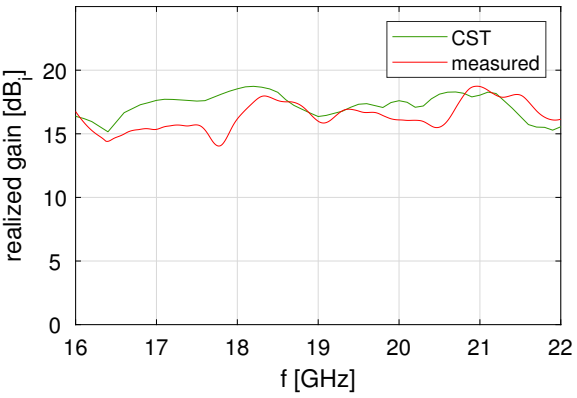

Fig. 16. Comparison between simulated and measured realized gain of the scanned beam versus frequency.

measured maximum realized gain of the structure. A good flat behavior and a very good agreement have been obtained over the entire frequency range. As already shown, Fig. 12 presents a comparison among the pointing directions of the main beam versus the frequency, considering two different LWAs as in Figs. 5, where the different probe positions and aperture sizes are compared. A very good agreement has been obtained among measurements and simulated values, as well as among simulations of the two structures and the leaky-wave models.

Figures 17(a)-(f) finally report a comparison among simu-

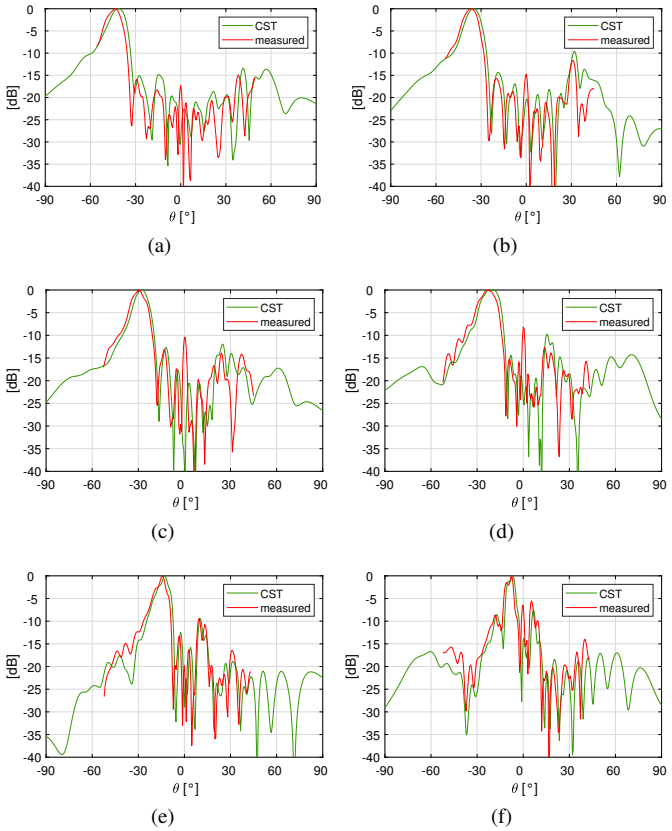

Fig. 17. Comparison among measured and simulated normalized radiation patterns along the main radial cut (containing one of the coaxial probes in Fig. 13, i.e., $\phi_s = 270°$), achieved activating port 1. From (a) to (f) the panels report six frequency values from 16 GHz (a) to 21 GHz (f).

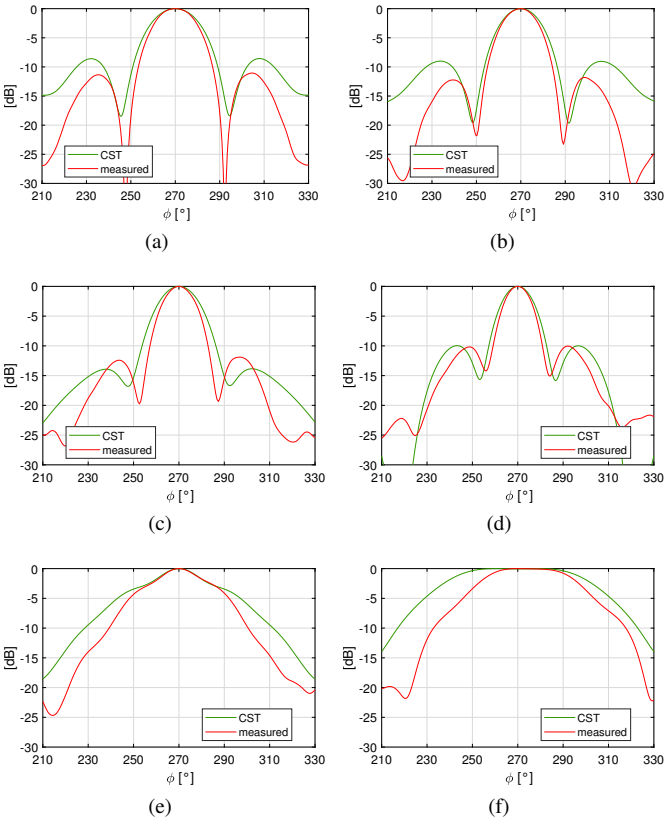

Fig. 18. Comparison among measured and simulated normalized radiation patterns along the azimuth cut at $\theta = \theta_p$ (given by the curve in Fig. 12), achieved activating port 1, as in Fig. 17. From (a) to (f) the panels report six frequency values from 16 GHz (a) to 21 GHz (f).

lated and measured radiation patterns over a radial cut containing one of the source presented in Fig. 13 (note that far-field measurements have been developed for both the ports giving essentially the same results; the plots report the beam patterns in the principal y-z plane when port 1 is driven). Six frequency values have been considered, from 16 GHz to 21 GHz, as in Fig. 8. The measured results have been reported from $-50°$ to $50°$, showing an excellent agreement with simulations both around the main direction and over the lateral regions. Figures 18(a)-(f) report the corresponding azimuth cuts at $\theta = \theta_p$, which is given in Fig. 12, showing a very good agreement among simulated and measured curves. The beam gradually loses directivity after 20 GHz, i.e., close to broadside, as also visible in Fig. 8.

V. Discussion and Conclusion

In this work we have discussed and demonstrated the possibility of generating a directional beam, scanning both in elevation and azimuth changing the frequency and the activated source of a circular multi-port system, respectively. This has been achieved by exciting an angularly tapered leaky-wave field distribution, associated with a fast backward spatial harmonic supported by a radially periodic two-dimensional multi-port leaky-wave antenna. A complete description of the design process and of the background physical mechanism has been given, along with numerical results for the dispersion analysis of the open planar waveguide. A practical feeding system has been designed and the radiation features of the beam have been tested by means of full-wave simulations performed on a commercial software tool. Far-field measurements have been reported on a prototype manufactured using standard printed-circuit technology.

The physical mechanism enabling the generation of the directional pencil beam has been assessed performing a GPOF analysis of the simulated aperture field. Thanks to the azimuthal symmetry, it has been seen that the proposed structure is able to successfully cover more azimuth directions, as many as the number of elements defining the multi-port system. The sources are anyway activated one at time, thus avoiding the need of lossy and cumbersome networks to phase them. By activating an additional source placed in the center of the structure it is also possible to reconfigure the system to radiate an omnidiretional conical pattern [33] scanning with the frequency, which could be used, e.g., to transmit a beacon signal for localization. Depending on the size constraints dictated by the application, higher values for the realized gain can be achieved by making larger the radial aperture of the antenna, which was constrained here by the size of the commercially available Taconic laminate.

The proposed antenna provides high radiation efficiency but, due to the exponential tapering of the aperture, has low aperture efficiency, of the order of 30% at the considered

working frequencies, which represents a common drawback for the leaky-wave antenna design. This feature as well as the level of the side lobes could be optimized by introducing a proper radial tapering of the attenuation constant of the leaky mode, which, thanks to the azimuthal symmetry of the structure and the excitation can still be applied in this case.

We have numerically investigated different structures (e.g., as those in [36]), which however would provide a narrower impedance bandwidth, with less satisfactory directional properties. It should be mentioned it is also possible to achieve similar results using a non-centered slot etched in the ground plane. These designs and the demonstrated prototype may represent an attractive low-cost solution for the generation of a directional beam over the 3-D space by means of a fully integrated and compact structure, which is a feature of increasing interest for several applications, such as indoor remote sensing and wireless powers transfer.

ACKNOWLEDGMENT

The Authors would like to thank Mr. Dejian Zhang at Tsinghua University for the help given to optimize the GPOF code.

REFERENCES

[1] R. J. Mailloux, *Phased Array Antenna Handbook*. Norwood, MA: Artech House, 2005, vol. 2.

[2] R. C. Hansen, *Phased Array Antennas*. Hoboken, NJ: John Wiley & Sons, 2nd ed., 2009.

[3] A. A. Oliner and D. R. Jackson, "Leaky-wave antennas," in *Antenna Engineering Handbook*, J. L. Volakis, Ed. New York, NY: McGraw-Hill, 2007, ch. 11.

[4] D. R. Jackson and A. A. Oliner, "Leaky-wave antennas," in *Modern Antenna Handbook*, C. A. Balanis, Ed. Hoboken, NJ: John Wiley & Sons, 2008, ch. 7, pp. 325–367.

[5] P. Baccarelli, P. Burghignoli, F. Frezza, A. Galli, and P. Lampariello, "Novel modal properties and relevant scanning behaviors of phased arrays of microstrip leaky-wave antennas," *IEEE Trans. Antennas Propag.*, vol. 51, no. 12, pp. 3228–3238, Dec. 2003.

[6] H. V. Nguyen, S. Abielmona, A. Rennings, and C. Caloz, "Pencil-beam full-space scanning 2D CRLH leaky-wave antenna array," in *2007 Int. Symp. on Signals, Systems and Electronics*, Jul. 2007, pp. 139–142.

[7] C.-C. Hu, C. Jsu, and J.-J. Wu, "An aperture-coupled linear microstrip leaky-wave antenna array with two-dimensional dual-beam scanning capability," *IEEE Trans. Antennas Propag.*, vol. 48, no. 6, pp. 909–913, Jun. 2000.

[8] M. Salarkaleji, M. A. Ali, and C.-T. M. Wu, "Two-dimensional full-hemisphere frequency scanning array based on metamaterial leaky wave antennas and feed networks," in *2016 IEEE MTT-S International Microwave Symposium*, 2016, pp. 1–4.

[9] D. Comite, P. Burghignoli, P. Baccarelli, and A. Galli, "2-D beam scanning with cylindrical-leaky-wave-enhanced phased arrays," *IEEE Trans. Antennas Propag.*, vol. 67, no. 6, pp. 3797–3808, Jun. 2019.

[10] J. R. Kelly and A. P. Feresidis, "Array antenna with increased element separation based on a Fabry–Perot resonant cavity with AMC walls," *IEEE Trans. Antennas Propag.*, vol. 57, no. 3, pp. 682–687, Mar. 2009.

[11] D. Blanco, N. Llombart, and E. Rajo-Iglesias, "On the use of leaky wave phased arrays for the reduction of the grating lobe level," *IEEE Trans. Antennas Propag.*, vol. 62, no. 4, pp. 1789–1795, Apr. 2014.

[12] F. Sultan and S. S. I. Mitu, "Superstrate–based beam scanning of a Fabry–Perot cavity antenna," *IEEE Antennas Wireless Prop. Lett.*, vol. 15, pp. 1187–1190, 2016.

[13] F. Costa, D. Bianchi, A. Monorchio, and G. Manara, "Linear Fabry-Perot/leaky-wave antennas excited by multiple sources," *IEEE Trans. Antennas Propag.*, vol. 66, no. 10, pp. 5150–5159, Oct. 2018.

[14] R. Gardelli, M. Albani, and F. Capolino, "Array thinning by using antennas in a Fabry–Perot cavity for gain enhancement," *IEEE Trans. Antennas Propag.*, vol. 54, no. 7, pp. 1979–1990, Jul. 2006.

[15] N. Llombart, A. Neto, G. Gerini, M. Bonnedal, and P. De Maagt, "Leaky wave enhanced feed arrays for the improvement of the edge of coverage gain in multibeam reflector antennas," *IEEE Trans. Antennas Propag.*, vol. 56, no. 5, pp. 1280–1291, May 2008.

[16] F. Scattone, M. Ettorre, B. Fuchs, R. Sauleau, and N. J. Fonseca, "Synthesis procedure for thinned leaky-wave-based arrays with reduced number of elements," *IEEE Trans. Antennas Propag.*, vol. 64, no. 2, pp. 582–590, Feb. 2016.

[17] D. Blanco, E. Rajo-Iglesias, A. M. Benito, and N. Llombart, "Leaky-wave thinned phased array in PCB technology for telecommunication applications," *IEEE Trans. Antennas Propag.*, vol. 64, no. 10, pp. 4288–4296, Oct. 2016.

[18] M. Poveda-García, D. Cañete-Rebenaque, and J. L. Gómez-Tornero, "Frequency-scanned monopulse pattern synthesis using leaky-wave antennas for enhanced power-based direction-of-arrival estimation," *IEEE Trans. Antennas Propag.*, vol. 67, no. 11, pp. 7071–7086, Nov. 2019.

[19] D. González-Ovejero, G. Minatti, G. Chattopadhyay, and S. Maci, "Multibeam by metasurface antennas," *IEEE Trans. Antennas Propag.*, vol. 65, no. 6, pp. 2923–2930, Jun. 2017.

[20] M. Bodehou, E. Martini, S. Maci, I. Huynen, and C. Craeye, "Multi-beam and beam scanning with modulated metasurfaces," *IEEE Trans. Antennas Propag.*, vol. 68, no. 3, pp. 2923–2930, Mar. 2020.

[21] D. Comite, S. K. Podilchak, P. Baccarelli, P. Burghignoli, A. Galli, A. P. Freundorfer, and Y. M. M. Antar, "Design of a polarization-diverse planar leaky-wave antenna for broadside radiation," *IEEE Access*, vol. 7, pp. 28 672–28 683, 2019.

[22] R. Guzmán-Quirós, J. L. Gómez-Tornero, A. R. Weily, and Y. J. Guo, "Electronically steerable 1-D Fabry–Perot leaky-wave antenna employing a tunable high impedance surface," *IEEE Trans. Antennas Propag.*, vol. 60, no. 11, pp. 5046–5055, Nov. 2012.

[23] L.-Y. Ji, Y. J. Guo, P.-Y. Qin, S.-X. Gong, and R. Mittra, "A reconfigurable partially reflective surface (PRS) antenna for beam steering," *IEEE Trans. Antennas Propag.*, vol. 63, no. 6, pp. 2387–2395, Jun. 2015.

[24] F. Costa and A. Monorchio, "Design of subwavelength tunable and steerable Fabry-Perot/leaky wave antennas," *Prog. Electromag. Res.*, vol. 111, pp. 467–481, 2011.

[25] R. Guzmán-Quirós, A. R. Weily, J. L. Gómez-Tornero, and Y. J. Guo, "A Fabry–Perot antenna with two–dimensional electronic beam scanning," *IEEE Trans. Antennas Propag.*, vol. 64, no. 4, pp. 1536–1541, Apr. 2016.

[26] T. Debogović and J. Perruisseau-Carrier, "Array-fed partially reflective surface antenna with independent scanning and beamwidth dynamic control," *IEEE Trans. Antennas Propag.*, vol. 62, no. 1, pp. 446–449, Jan. 2014.

[27] M. U. Afzal and K. P. Esselle, "Steering the beam of medium–to–high gain antennas using near-field phase transformation," *IEEE Trans. Antennas Propag.*, vol. 65, no. 4, pp. 1680–1690, Apr. 2017.

[28] A. Lalbakhsh, M. U. Afzal, K. P. Esselle, and S. L. Smith, "Wideband near-field correction of a Fabry–Perot resonator antenna," *IEEE Trans. Antennas Propag.*, vol. 67, no. 3, pp. 1975–1980, Mar. 2019.

[29] B. Ratni, W. A. Merzouk, A. de Lustrac, S. Villers, G.-P. Piau, and S. N. Burokur, "Design of phase-modulated metasurfaces for beam steering in Fabry–Perot cavity antennas," *IEEE Antennas Wireless Propag. Lett.*, vol. 16, pp. 1401–1404, 2017.

[30] A. Ip and D. R. Jackson, "Radiation from cylindrical leaky waves," *IEEE Trans. Antennas Propag.*, vol. 38, no. 4, pp. 482–488, Apr. 1990.

[31] D. Comite, P. Burghignoli, P. Baccarelli, D. Di Ruscio, and A. Galli, "Equivalent-network analysis of propagation and radiation features in wire-medium loaded planar structures," *IEEE Trans. Antennas Propag.*, vol. 63, no. 12, pp. 5573–5585, Dec. 2015.

[32] D. Comite, P. Baccarelli, P. Burghignoli, and A. Galli, "Omnidirectional 2-D leaky–wave antennas with reconfigurable polarization," *IEEE Antennas Wireless Propag. Lett.*, vol. 16, pp. 2354–2357, 2017.

[33] D. Comite, V. Gómez-Guillamón Buendía, S. K. Podilchak, D. Di Ruscio, P. Baccarelli, P. Burghignoli, and A. Galli, "Planar antenna design for omnidirectional conical radiation through cylindrical leaky waves," *IEEE Antennas Wireless Propag. Lett.*, vol. 17, no. 10, pp. 1837–1841, 2018.

[34] D. Comite, W. Fuscaldo, S. Podilchak, P. D. Hilario Re, V. Gómez-Guillamón Buendía, P. Burghignoli, P. Baccarelli, and A. Galli, "Radially periodic leaky-wave antenna for Bessel beam generation over a wide-frequency range," *IEEE Trans. Antennas Propag.*, vol. 66, no. 6, pp. 2828–2843, Jun. 2018.

[35] S. K. Podilchak, P. Baccarelli, P. Burghignoli, A. P. Freundorfer, and Y. M. M. Antar, "Optimization of a planar bull-eye leaky-wave antenna fed by a printed surface-wave source," *IEEE Antennas Wireless Propag. Lett.*, vol. 12, pp. 665–669, 2013.

[36] ——, "Analysis and design of annular microstrip-based planar periodic leaky-wave antennas," *IEEE Trans. Antennas Propag.*, vol. 62, no. 6, pp. 2978–2991, Jun. 2014.

[37] Y. Hua and T. K. Sarkar, "Generalized pencil-of-function method for extracting poles of an EM system from its transient response," *IEEE Trans. Antennas Propag.*, vol. 37, no. 2, pp. 229–234, Feb. 1989.

[38] A. Singh, R. Paknys, and D. R. Jackson, "Using the matrix pencil method to analyze a 3D leaky wave antenna," in *2015 IEEE International Symposium on Antennas and Propagation & USNC/URSI National Radio Science Meeting*. IEEE, 2015, pp. 23–24.

[39] S. Paulotto, P. Baccarelli, F. Frezza, and D. R. Jackson, "A novel technique for open-stopband suppression in 1-D periodic printed leaky-wave antennas," *IEEE Trans. Antennas Propag.*, vol. 57, no. 7, pp. 1894–1906, Jul. 2009.

[40] S. Otto, A. Al-Bassam, A. Rennings, K. Solbach, and C. Caloz, "Transversal asymmetry in periodic leaky-wave antennas for Bloch impedance and radiation efficiency equalization through broadside," *IEEE Trans. Antennas Propag.*, vol. 62, no. 10, pp. 5037–5054, Jul. 2014.